COMSOL CONFERENCE 2025 AMSTERDAM

Assessment of hydrodynamic forces on a moving piston in a submerged cylinder

K. Rezk[1], W. Lin[1], J. Forsberg[1,2]
1. Department of engineering and chemical sciences, Karlstad University, Karlstad, Sweden
2. Waves4power AB, Gothenburg, Sweden

Abstract
The WaveEL buoy is characterized as a point absorber and has a 36 meters long vertical cylinder where a water piston is oscillating due to induced motion from the waves. Estimating the wave loads on the piston is a challenge due to the presence of adjacent cylinder walls. The narrow leakage width between the piston and the cylinder walls presents a phase shift to the relative motion of the oscillating water flow and the piston. Understanding and characterizing the phase angle is important in order to estimate added mass and damping in the water piston. The WaveEL buoy is analyzed with a 2-dimensional axial symmetric representation. The k-ω turbulence model is used to simulate the water domain and the solid mechanics model, through fluid-solid interaction coupling, is used to simulate the displacement of the piston. The phase angle between hydrodynamic forces and mean water flow in the submerged cylinder is estimated using sample covariance. Leakage widths at 1, 2, 3, 5, 7, 10, 15 and 25 cm were simulated for a periodic pulse with a force amplitude of 100 kN and a time period of 6.28s. The hydrodynamic coefficients are assessed and correlations between the Keulegan-Carpenter number and added mass coefficient as well as the Reynolds number and the added damping coefficient were deduced and assessed. Initial findings suggest that added mass decrease with increased leaking widths due to a loss in acceleration of the water mass. Moreover, added damping is also reduced which indicates lower power uptake as a result of the reduced C_d-coefficient.

Keywords: CFD, wave power, FSI, point-absorber, added mass, added damping

Introduction
Point Absorbers (PAs) are devices that extract energy from the relative motion between a floating or submerged body and a fixed structure. These components, which may be anchored at various depths, generate electricity through the oscillating motion of waves [1]. One advantage of PAs is their typically small size relative to the incident wavelength, allowing them to absorb energy efficiently from waves coming in any direction. This contributes to more continuous and reliable power output [2]. Various hydrodynamic models have been developed to analyze PA performance. These models are generally categorized as linear potential flow models, weakly nonlinear Froude–Krylov methods, or fully nonlinear models. The unsteady Navier–Stokes (NS) equations, part of the nonlinear modeling class, are used in this study. Wave excitation forces on floating cylinders have been widely investigated, with several studies applying nonlinear numerical models to simulate extreme wave conditions. These models have been validated experimentally with high accuracy [3, 4].

Research has been conducted on submerged objects undergoing heaving motion, where the Volume of Fluid (VOF) method is used to simulate interactions between solid structures and water [5-8]. However, these studies typically analyze scenarios far from any wall effects. There is limited research on hydrodynamic force characterization of submerged objects with heaving motion in internal oscillating flow systems—a gap that this study aims to address.

The buoy WaveEL that this paper is investigating is a wave energy converter (WEC) of the sort PA with an eight meter in diameter buoy with a 36m long vertical tube submerged in the water. The flow around the water piston is complex and varies in time by shifting from laminar to turbulent phases creating vortex shedding for instance. CFD-analysis of the flow is a way to get better knowledge of flow-pattern around, and of pressure drop across the water piston. Due to increased manufacturing demands on piston edge preciseness as well as positioning around its axis as a result of narrow leakage widths, a better understanding of piston and water motion and resulting hydrodynamic forces is needed to make proper decisions on the design in terms of manufacturing costs as well as energy performance of the buoy.

A Simulink model of WaveEL-system where power output is calculated based on tube flow, water surface level and water-piston motion were developed by [9] and is thoroughly described in [10]. The current lumped system model of the WaveEL buoy roughly considers hydrodynamic forces based on averaged values of coefficients representing

added mass and damping. A clear understanding of the dynamic loading on the piston is essential for accurately predicting end-stop impacts on bumpers in the cylinder, which is a key factor in the design of more robust and sustainable wave energy converters. In order to both consider bumper impact as well as power uptake through the water-piston, added mass and added damping have to be properly assessed.

A 2-dimensional axial symmetric representation of the WaveEL submerged tube and water piston was set up and analyzed using a fluid structure interaction (FSI) model based on the transient k-ω turbulence model. The purpose of this paper is to improve the understanding of WaveELs performances and the aim is to better understand how leakage flow around the piston influences the hydrodynamic forces and, ultimately, energy conversion efficiency. Further analysis will aim to find correlations and expressions of the KC-number to added mass, as well as the Re-number for added damping, for different leakage widths. By doing so, a better description of the coupling motion of the water piston and tube water can be made in the lumped system model which could provide better assessment of power uptake and bumper force impact.

Theory / Numerical Set Up

The procedure of the method involves a brief presentation of the buoy system, numerical model setups and a framework of how the hydrodynamic forces and velocities/acceleration are calculated and assessed.

WaveEL – system

The Waves4Power WaveEL system is a point absorber consisting of a buoy with a diameter of eight meters and a 36-meter-long vertical tube passing through its center (see Fig. 1). This vertical structure, referred to as the acceleration tube, extends approximately 34 meters below the sea surface and is open at both ends. Inside the acceleration tube floats a water piston that drives the power take-off (PTO) system, which operates using a hydraulic motor. The piston and water oscillate within a designated stroke proximately four meters in length. A small gap, known as the leakage width, exists between the piston and the inner wall of the tube. The buoy is secured in position by mooring lines, which provide stability while still allowing vertical movement to accommodate wave dynamics. Electrical energy generated by the system is transmitted via dynamic cables to a subsea connection hub, and from there through subsea cables to the end user. [9]

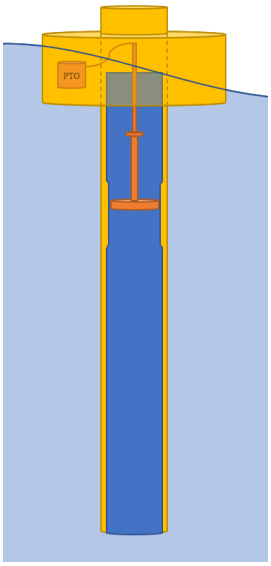

Figure 1. Schematic view of WaveEL. [11]

The WaveEL system can be modeled as comprising two distinct masses: the first is the buoy and the attached acceleration tube, and the second is the water column inside the tube. Incoming waves influence these two masses differently, causing them to oscillate with different natural frequencies and thus move out of phase with one another. The power take-off (PTO) system is designed to harness this relative motion. By damping the movement of the internal piston—which responds to the difference in motion between the two masses—the system works to bring them closer to phase alignment. In doing so, it captures the excess mechanical energy from their relative motion and converts it into electrical energy.

Geometry properties

The modelling procedure includes transient analysis on the relation of the hydrodynamic force on the piston and the tube water velocity. The procedure involves the implementation of a fluid flow model and a structural mechanics model with a moving mesh of the piston in the tube domain so that the relative motion of the water and the piston is studied. Key geometrical features of the buoy can be found in [10]. For simplicity, the expansion area in water tube is not included in the analysis. However, the correct water mass must be accounted for in the simulations to ensure the proper inertia in the computational domain. In turn, the length of the tube is increased to 40.24 m from its original length of 36 m.

Governing Equations

The unsteady, incompressible flow field was simulated with the time-averaged Navier-Stokes equations (RANS) with a k-ω turbulence closure model.

$$\frac{\rho\partial \boldsymbol{u}}{\partial t} + \rho(\boldsymbol{u}\cdot\nabla)\boldsymbol{u} = \nabla[-p\boldsymbol{I} + ((\mu+\mu_T)(\nabla\boldsymbol{u} + (\nabla\boldsymbol{u})^T)] + \boldsymbol{F} + \rho\boldsymbol{g} \quad (1)$$

$$\rho\nabla\cdot\boldsymbol{u}=0 \quad (2)$$

$$\frac{\rho\partial k}{\partial t}+\rho(\boldsymbol{u}\cdot\nabla)k=P_k-\rho\beta_0^*k\omega+\nabla[(\mu+\sigma_k\mu_T)\nabla k] \quad (3)$$

$$\frac{\rho\partial\omega}{\partial t}+\rho(\boldsymbol{u}\cdot\nabla)\omega=\alpha\frac{\omega}{k}P_k-\rho\beta\omega^2+\nabla[(\mu+\mu_T\sigma_\omega)\nabla\omega] \quad (4)$$

The structural mechanics formulation describes the deformation of solid bodies under the influence of internal and external loads. In the context of fluid–structure interaction (FSI), the structural domain is dynamically coupled to the surrounding fluid, leading to a two-way exchange of momentum and displacement.

FSI coupling appear on the boundaries between the piston and the water mass. The FSI is based on the Arbitrary Lagrangian-Eulerian (ALE) method where the fluid flow is described in a Eulerian spatial frame of reference and the piston with a Lagrangian material frame of reference. The FSI coupling only considers force transmission between the piston and water, hence the stress field and deformation of the piston is not of any interest in this study. The total force exerted on the piston boundary by the fluid is the negative of the reaction force on the fluid

Numerical Model

A 2-dimensional axial-symmetric reference frame was used to observe the motion of the piston and water mass. The piston is set in motion due to the exposed forces transmitted from the buoy. This is modeled by applying a sinusoidal volume force source term representing the load from the waves, see Fig. (2). Gravity and buoyancy forces are excluded from the simulations as they only act as bias. Hence, the hydrodynamic forces on the piston surface as well as added mass are analyzed in relation the piston load.

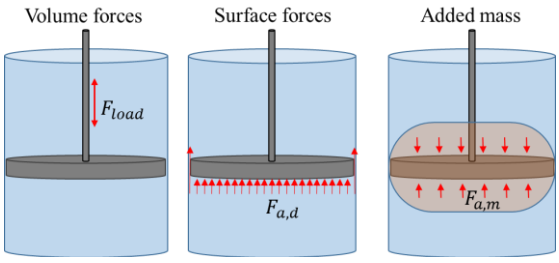

Figure 2. Schematic representation of forces in the water piston.

Standard material properties for water were used with a modification of the density to resemble salt water.

Initial and boundary conditions

Initially, the piston is centered in the acceleration tube, see Fig. (3). The acting forces are modelled as a sinus-function which benefits potential initial value problems and insure stability in the solution. The no-slip conditions were applied at all solid boundaries, the axial-symmetry conditions are applied at the vertical boundary at r = 0, which is the axis of rotation. Open boundary is set on the top boundary. An inlet boundary is set at the bottom boundary where constitutional variables of velocity field (u_{fluid}, w_{fluid}) are used so that water can be transported in and out due to the movement of the buoy.

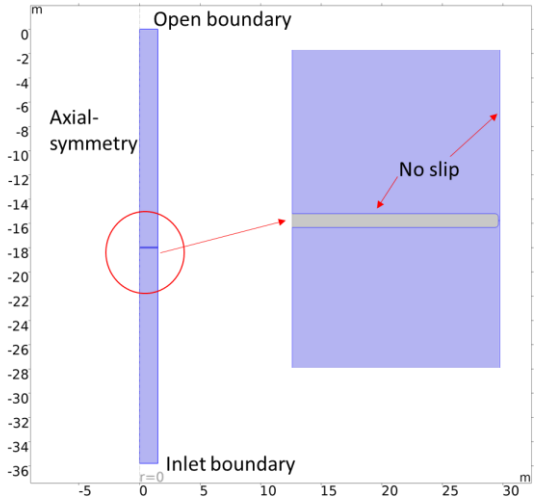

Figure 3. 2-dimensional representation of water piston and submerged cylinder in Comsol with boundary conditions.

Simulation trials

A sinusoidal volume force term is applied in the piston with an amplitude of 100 kN and a time period of 2π s, see Eq. (5).

$$F_{load}(t)=F_0\sin(\omega t) \quad (5)$$

The piston and water motion are analysed for leakage widths 1, 2, 3, 5, 7, 10, 15 and 25cm, see Fig. (4).

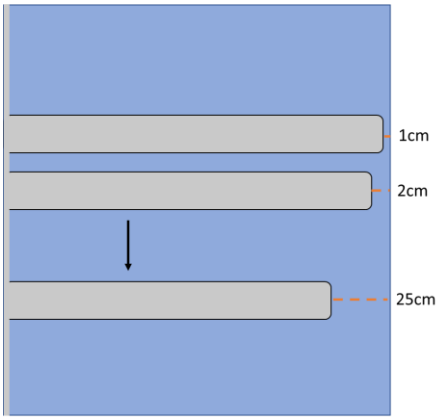

Figure 4. Schematic presentation of different leaking widths.

Different data was probed during the simulations and are summarized in Table (1). The data is exported to MATLAB for further analysis.

***Table 1**: Key input data to the simulation model*

Output data	Unit	Method
F_{hydro}	[kN]	Surface integration
w_{water}	[m/s]	Volume average
w_{piston}	[m/s]	Volume average
$w_{leakage}$	[m/s]	Line average
$\dot{w}_{water}$	[m/s^2]	Volume average
$\dot{w}_{piston}$	[m/s^2]	Volume average
z_{piston}	[m]	Line average

CFD data analysis in MATLAB

For oscillating flow problems, the resulting forces is function of velocity and acceleration. The phase shift of the viscous contribution in the resulting force can be depicted as in Fig. (5) where the drag force is in the same direction as water velocity.

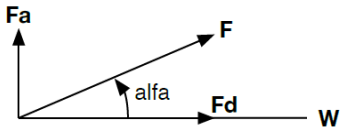

Figure 5. Hydrodynamic forces on the piston.

The dynamic relation between the motion of and the force on the water piston may be assessed through covariance analysis in the time domain, see Eq. (6)

$$K_{XY}(\tau) = E[X_t, Y_{t-\tau}] - \mu_X \mu_Y \quad (6)$$

where the maximum/minimum value of $K_{XY}(\tau)$ is determined by τ and the sampling frequency. In the case of Eq. (6), the velocity of the water mass is reference time series (X_t). The phase angle of the interactive force between the moving water-piston and tube-water is assessed by estimating the phase angle of forces related to drag (pressure and friction forces) and inertia (acceleration).

$$F_{a,d} = F_{hydro} \cdot \cos(K_{XY}) \quad (7)$$
$$F_{a,m} = F_{hydro} \cdot \sin(K_{XY}) \quad (8)$$

These force components are categorized as added damping and added mass and are presented in Eq. (9) and (10).

$$F_{a,d} = C_d \rho A \frac{\widehat{w_{rel}}^2}{2} \quad (9)$$

$$F_{a,m} = m_{add}(1 + KC)\widehat{\dot{w}_{rel}} \quad (10)$$

V_{ref} for a thin plate such as the piston for theoretically ideal external flow problems is defined as

$$V_{ref} = \frac{D_h^3}{3} \quad (11)$$

where D_h is the characteristic length which is the piston diameter. The characteristic velocity for this particular flow problem is chosen as the average of the maximum and minimum relative velocity difference of the piston and water mass.

$$w_{rel} = w_{piston} - w_{water} \quad (12)$$

$$\widehat{w_{rel}} = \frac{max(w_{rel}) - min(w_{rel})}{2} \quad (13)$$

For oscillating flow, the added mass relates the inertial force term with the acceleration of the moving object. For the case in this study, the relative acceleration of the piston and water mass was taken into consideration in which the average value of maximum and minimum value of relative acceleration was used.

$$\dot{w}_{rel} = \dot{w}_{piston} - \dot{w}_{water} \quad (14)$$

$$\widehat{\dot{w}}_{rel} = \frac{max(\dot{w}_{rel}) - min(\dot{w}_{rel})}{2} \quad (15)$$

Non-dimensional numbers in oscillating flow

There are classical methods to use in the analysis of forces on blunt bodies in stagnant fluids such using inertia and viscosity to estimate force-interactions between a blunt body and the surrounding fluid. Keulegan-Carpenter (KC) number and Reynolds (Re) number are used to assess the forces. The KC-number is related to the Navier-Stokes equation through the acceleration terms which are approximated according to Eq. (16) and (17).

$$Convective: (u \cdot \nabla u) \sim \frac{U^2}{L} \quad (16)$$
$$Local: \frac{\partial u}{\partial t} \sim \frac{U}{T} \quad (17)$$

The ratio between the two expressions defines the KC-number which also describes the relative importance of drag forces (U^2) and inertia forces (U/T)

$$KC = \frac{UT}{2\pi D_h} \quad (18)$$

The Re number is the standard expression with the characteristic length set to piston diameter divided by 4.

$$Re = \frac{U \cdot D_h}{4\nu} \quad (19)$$

In fluid mechanics, the term added mass refers to the additional inertia experienced by a body as it accelerates or decelerates, since it must also set a portion of the surrounding fluid into motion (or displace it) while moving through it. The added mass relates the acceleration of the water mass to inertial

force component and can be determined through Eq. (20).

$$m_{add} = \frac{F_{a,m}}{(1+KC)\widetilde{w_{rel}}} \quad (20)$$

The drag and added mass coefficient can be determined from Eq. (21) and (22).

$$C_d = \frac{8F_{a,d}}{U^2\pi D_h^2} \quad (21)$$

$$C_m = \frac{m_{add}}{\rho V_{ref}} \quad (22)$$

The analysed data is summarised in Table. (2) and is presented in the paragraph "Results and Discussion".

***Table 2**: Summary of hydrodynamic data on the water-piston/cylinder system*

Output data	Unit
F_d	[kN]
F_m	[kN]
C_d	[-]
C_m	[-]
m_{Add}	[ton]
Re	[-]
KC	[-]

Mesh setup and solver settings

An unstructured mesh grid containing triangle elements was created for the piston-cylinder model. The grid is solved in a finite element space where a set of basis functions are used to create piecewise linear relations between the mesh elements and convert them to weak formulations for them to be solved. Comsol´s physics-based mesh settings were used with a coarser configuration resulting in a total number of elements at approximately 18500. Further analysis will focus on mesh sensitivity as it is deemed crucial for the objective data of this study.

The output times in the time-dependent solver are set according to Eq. (23)

$$t \in [0, 3 \cdot \pi] \quad (23)$$

where the sample frequency is 100 Hz.

A direct linear system solver was used coupled with an implicit second order backward differentiation formula (BDF) solver. The direct solver is called PARDISO which handles sparse linear systems using LU factorization to compute a solution. More information on the solver is found in COMSOL documentation. The BDF solver performs time stepping using a backward differentiation with a maximum order of accuracy of 2, which is the degree of the interpolating polynomial.

In simulations involving large deformations with moving boundaries, the computational mesh may become highly distorted and lead to numerical instabilities. The automatic remeshing feature is used to account for the moving mesh of the piston and its surroundings that allow the mesh to be regenerated during the simulation. The remeshing process uses mesh quality as a condition.

Results and Discussion

The analysed CFD data from the numerical runs for all leaking widths are summarized in Table (3).

***Table 3**: Summary of hydrodynamic data on the water-piston/cylinder system*

L_w [cm]	F_d [kN]	F_m [kN]	KC	C_m	m_{Add} [ton]	Re	C_d
1	96.16	5.78	0.23	55.1	63.6	3.3e4	1.4e4
2	95.82	9.61	0.55	33.3	37.6	7.6e4	2.6e3
3	96.13	8.67	0.79	19.0	21.1	1.1e5	1.3e3
5	96.23	8.69	1.25	10.2	10.9	1.7e5	543.6
7	95.95	10.59	1.72	7.75	7.91	2.2e5	299.1
10	96.34	11.62	2.46	4.85	4.65	3.1e5	160.5
15	98.15	7.87	3.45	1.77	1.69	4.3e5	83.1
25	97.03	4.85	5.84	0.67	0.46	5.8e5	44.8

Some clear trends can be observed from data such as increased Re- and KC number with increased leaking widths as a result from a higher relative velocity difference between the piston and the water mass, see Fig. (6) and (7). For that same reason, the drag and added mass coefficient are reduced with increased leaking widths.

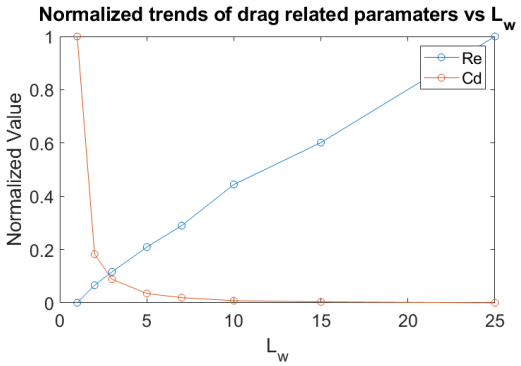

Figure 6. Normalized values of the Re-number and the drag coefficient for all leaking widths

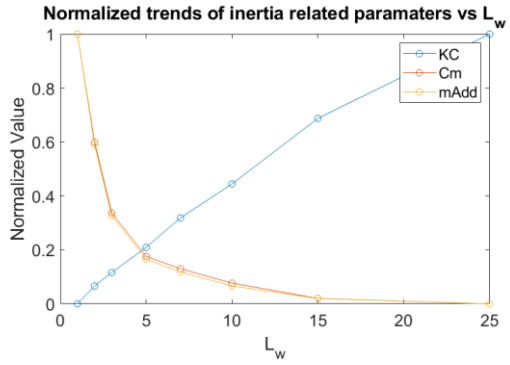

Figure 7. Normalized values of the KC-number and the added mass coefficient for all leaking widths.

The hydrodynamic force, piston displacement, piston and tube water velocity, as well as the relative acceleration between the piston and water mass, are presented in Fig. (8) – (10). The results reveal that increasing the leakage width amplifies the difference between piston velocity and water velocity. For small leakage (1 cm), piston and water velocities remain closely aligned, whereas for larger leakage widths (10 cm and 25 cm) the water velocity deviates substantially, such that the relative velocity approaches the piston velocity.

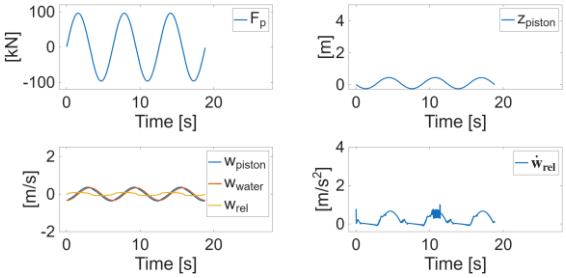

Figure 8. Hydrodynamic force, piston displacement, piston and tube water velocity as well as relative acceleration of the piston and water mass for 1 cm leaking width.

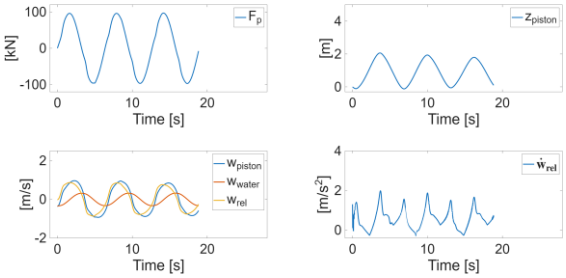

Figure 9. Hydrodynamic force, piston displacement, piston and tube water velocity as well as relative acceleration of the piston and water mass for 10 cm leaking width.

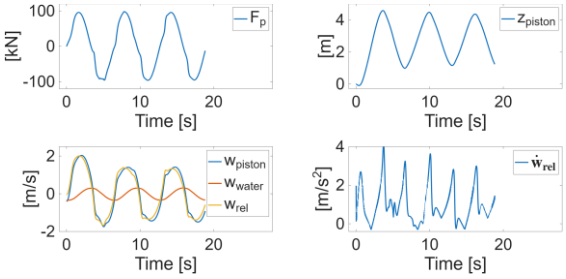

Figure 10. Hydrodynamic force, piston displacement, piston and tube water velocity as well as relative acceleration of the piston and water mass for 25 cm leaking width.

This trend explains the observed increase in Reynolds and Keulegan–Carpenter numbers with increasing leakage width to Eq. (18) and (19) and the corresponding decrease in drag and added mass coefficients Eq. (21) and (22).

In order to make results more scalable, the drag and added mass coefficients are expressed as a function of the Re- and KC number respectably, see Fig. (11).

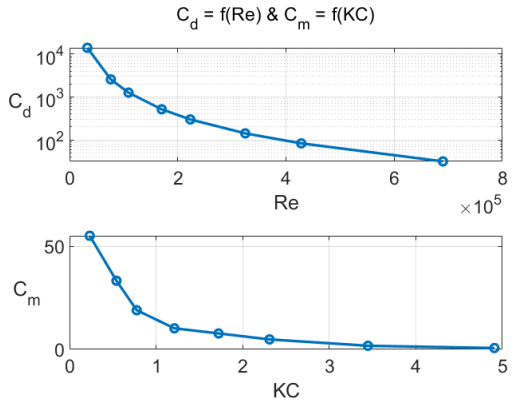

Figure 11. The drag and added mass coefficient as function of the Re- and KC-number respectively. Each circle mark represents the leaking width.

In the top panel, the C_d-coefficient exhibits a strong inverse dependence on Re-number. At low Reynolds numbers, the drag coefficient is very high ($C_d \sim 4e^4$), reflecting the dominance of viscous forces in the flow regime. As Re-number increases, inertial effects become more significant, leading to a rapid reduction in C_d. The curve begins to flatten at higher Re-numbers which is consistent with classical hydrodynamic behavior, where the drag coefficient approaches an asymptotic value at high Reynolds numbers. In the bottom panel of Fig. (11), the inertia coefficient C_m decreases sharply with increasing KC. At small values of KC (< 0.5), C_m reaches values above 50, highlighting those inertial forces dominate over drag in oscillatory flows with limited displacement. However, as KC increases, C_m rapidly declines, approaching zero for KC > 3. This indicates a transition toward drag-dominated regimes, where fluid particle displacement over a cycle becomes large relative to the body dimension.

Taken together, the results demonstrate the contrasting roles of viscous drag and inertial effects under different flow regimes. High Re flows minimize drag effects, while high KC flows diminish the relative contribution of inertia. For leaking widths at 25cm or more, the behavior of the drag and added mass coefficient transitions towards a more traditional external flow problem (heave motion

without tube walls) where vortex shedding so more decisive and has a negative affect on the power uptake from the piston. Such insights are crucial for modeling hydrodynamic forces in oscillatory or unsteady flows, particularly in applications involving offshore structures.

Conclusions

A 2-dimensional axisymmetric FSI model of the WaveEL buoy was developed to investigate how leakage flow around the piston affects hydrodynamic forces and, by extension, energy conversion efficiency. The results show that increasing leakage width enhances the relative velocity between piston and water, leading to higher Reynolds and Keulegan–Carpenter numbers and a corresponding reduction in drag and added mass coefficients. By expressing these coefficients as functions of Reynolds and KC numbers, scalable relationships were established that capture the transition between inertia- and drag-dominated regimes.

These insights provide a more accurate description of the coupled motion of the piston and tube water, offering improved inputs for lumped system models of WaveEL. Ultimately, this contributes to more reliable assessments of power uptake and bumper force impact, thereby supporting the overall goal of optimizing energy conversion efficiency in wave energy systems.

Acknowledgements

The authors are grateful for the support from Waves4power in terms of input and configuration data as well as providing valuable feedback to the project.

References

[1] Aderinto T, Li H. Ocean Wave Energy Converters: Status and Challenges. Energies. 11(5) (2018).
[2] He GH, Luan ZX, Zhang W, He RH, Liu CG, Yang KB, et al. Review on research approaches for multi-point absorber wave energy converters. Renew Energ. 218 (2023).
[3] Katsidoniotaki E, Shahroozi Z, Eskilsson C, Palm J, Engström J, Göteman M. Validation of a CFD model for wave energy system dynamics in extreme waves. Ocean Eng. 268 (2023).
[4] Sjökvist L, Wu JM, Ransley E, Engström J, Eriksson M, Göteman M. Numerical models for the motion and forces of point-absorbing wave energy converters in extreme waves. Ocean Eng. 145 (2017).
[5] Anbarsooz M, Passandideh-Fard M, Moghiman M. Numerical simulation of a submerged cylindrical wave energy converter. Renew Energ. 64 (2014).
[6] Rafiee A, Fiévez J. Numerical Prediction of Extreme Loads on the CETO Wave Energy Converter. Proceedings of the 11th European Wave and Tidal Energy; Nantes, France2015.
[7] Zan XX, Lin ZH. On the applicability of Morison equation to force estimation induced by internal solitary wave on circular cylinder. Ocean Eng. 198 (2020).
[8] Zan XX, Lin ZH, Gou Y. Numerical study on the force distribution on cylindrical structure by internal solitary wave and its prediction with Morison equation. Ocean Eng. 248 (2022).
[9] Waves4power. Waves4power; https://www.waves4power.com/waves4power-the-solution.
[10] Zeinali S, Wiktorsson M, Forsberg J, Lindgren G, Lindström J. Optimizing the hydraulic power take-off system in a wave energy converter.
[11] Tebelius L. Multidisciplinary Modelling of Water Piston Oscillations in Wave Energy Converters: Karlstad University; 2022.